



Nanoscale zero-valent iron (nZVI) synthesis in a Mg-aminoclay solution exhibits increased stability and reactivity for reductive decontamination



Yuhoon Hwang ^{a,*}, Young-Chul Lee ^{b,c,**}, Paul D. Mines ^a,
Yun Suk Huh ^c, Henrik R. Andersen ^a

^a Department of Environmental Engineering, Technical University of Denmark, Miljøvej, B113, DK-2800 Kgs. Lyngby, Denmark

^b Department of Civil and Environmental Engineering, KAIST, 291 Daehak-ro, Yuseong-gu, Daejeon 305-701, Republic of Korea

^c Department of Biological Engineering, College of Engineering, Inha University, Incheon 402-751, Republic of Korea

ARTICLE INFO

Article history:

Received 19 August 2013

Received in revised form 1 October 2013

Accepted 7 October 2013

Available online 16 October 2013

Keywords:

Mg-aminoclay (MgAC)

Nanoscale zero-valent iron (nZVI)

Nanotechnology

Colloidal stability

ABSTRACT

Nanoscale zero-valent iron (nZVI) has often been explored as a reductant for detoxification of pollutants in environmental clean-ups. Despite the large surface area and superior reactivity of nZVI, its limited stability is a major obstacle in applying nZVI for in situ subsurface remediation, e.g. for chlorinated solvents hotspots. In this study, water-solubilized magnesium-aminoclay (MgAC) was applied for the first time as a stabilizing agent in the synthesis of nZVI. With increased doses of Mg-aminoclay applied in the synthesis mixture, nZVI particle growth was inhibited and thin sheathed grape-like nZVI particles with higher crystallinity were produced. Stability of nZVI particles were evaluated using a sedimentation test and a dynamic light scattering technique. The characteristic time increased from 6.71 to 83.8 min, and particle (aggregate diameter) size decreased from 5132 to 186 nm with increasing amounts of applied MgAC. The higher stability of MgAC coated nZVI could be explained from the higher zeta potential, which indicates that the stabilization mechanism is increased electrostatic repulsion from the positively charged MgAC coating. The optimal weight ratio between MgAC and iron was found to be 7.5:1. The MgAC coated nZVI exhibited higher reactivity for nitrate reduction with the observed first order rate constants increasing from 1.17 to 42.0 h⁻¹, and Fe(0)-normalized rate constants from 0.124 to 43.8 h⁻¹ mg-Fe(0)⁻¹. Consequently, the MgAC coated nZVI showed increased feasibility, compared to uncoated nZVI, for application in remediation of subsurface contaminations; where high stability and mobility as well as high reactivity for degradation of contaminants is desired.

© 2013 Elsevier B.V. All rights reserved.

1. Introduction

Applications of zero valent iron (ZVI) have emerged as one of the most innovative technologies for water treatment and soil/groundwater remediation processes [1]. Due to its suitable redox potentials, it has been applied to the removal of a wide variety of pollutants, including chlorinated hydrocarbons, nitrobenzenes, chlorinated phenols, polychlorinated biphenyls (PCBs), heavy metals, and various anions [2]. In particular, with its small size and high specific surface area, nanoscale zero valent iron (nZVI) is a promising and flexible technology for in situ remediation of

groundwater contaminants that are amenable to reduction by electron donation of ZVI [3].

To be effective for in situ subsurface remediation, nZVI particles must be stable against aggregation; otherwise their mobility in groundwater will be greatly limited. However, uncoated nZVI particles tend to rapidly agglomerate due to van der Waals forces and magnetic attraction, rendering them undeliverable to the locations where the targeted contaminant is found [4,5]. This results in both limited stability and mobility of nZVI in aqueous solution and the subsurface environment. Phenrat et al. [6] reported that a cluster size of 70 μm could be reached in 30 min, even though the primary particle size was 20 nm during nZVI synthesis in aqueous solutions, where uncoated nZVI could migrate only up to few meters from the point of injection [7,8].

Thus, to prevent aggregation of metallic nanoparticles, particle stabilization has been achieved in many studies by attaching stabilizing molecules onto the nanoparticles [5]. The stabilizing agents, such as anionic or nonionic surfactants [9,10],

* Corresponding author. Tel.: +45 5065 7851; fax: +45 4593 2850.

** Corresponding author. Tel.: +82 42 350 3610; fax: +82 42 350 3698.

E-mail addresses: yuoh@env.dtu.dk (Y. Hwang), dreamdbs@kaist.ac.kr (Y.-C. Lee).

sodium carboxymethyl cellulose [4,11], starch [12,13], and guar gum [14], are designed to provide strong interparticle electrostatic and/or steric repulsions to overcome the attractive forces of nZVI or other metallic nanoparticles.

Over the past decades, as an alternative to organic stabilizing agents, natural clay minerals have been applied as a host matrix or support material to synthesize metallic nanoparticles; due to their potential applications in catalysis and other functional composites, mainly by intercalation into the interfacial layers [15–17]. During the synthesis of metallic nanoparticles, layered structures of inorganic clays work as a nano-sized reactor, to produce confined environments or grant dispersion ability as a stabilizing agent. The unique structural properties of clay minerals control the nucleation of clusters and limit particle growth; consequently, this process is considered a pre-synthesis stabilization approach. For example, Jia and Wang reported the successful synthesis of stable sub-nano-sized montmorillonite-supported nZVI (0.5 nm), indicating that the clay matrix was suitable to aid in dispersion and size reduction of nZVI particles [16].

In 1997, organo-functionalized clays were first described, using new direct synthesis routes applying the sol-gel process under ambient conditions [18–20]. With this method, simple hybrid phyllosilicate clays were introduced with the copolymerization of magnesium ions and trialkoxysilanes under alkaline catalysts at moderate temperature [21,22]. As a representative, aminosilanes employed hybrid phyllosilicates clay, called aminoclays, were produced autocatalytically with no need of base catalysts during the synthesis reaction [23]. Particularly, Mg-based materials with 3-aminopropyltriethoxysalane, composed of a Mg-occupied octahedral sheet sandwiched between two tetrahedral silica layers in the unit structure, has been shown to have multiple applications. Ongoing uses are reported for self-assembled bio-nanocomposites [18,24–26], microalgae-based biorefineries [27–30], and environmental clean-ups [31–34] using the unique properties of MgAC in aqueous solution.

Organic-functional groups of $-(CH_2)_3NH_2$, in tetrahedral sheets of MgAC, are protonated to form positively charged $-NH_3^+$ ions. The delaminated organo-building blocks of MgAC showed an average hydrodiameter of approximately 50 nm, due to a strong electrostatic repulsion of each clay sheet [35]. Importantly, MgAC showed superior water-solubility and high transparency in concentrations up to 100 g/L in aqueous solution [31]. These positively charged organo-building blocks of MgAC in aqueous solution could offer a template for synthesis of metallic nanoparticles or as stabilizing agents [36–38]. Recently, noble metal nanoparticles such as Pt, Pd, Ag, and Au, were successfully synthesized by chemical reduction in the presence of MgAC [39]. In addition, copper metal particles were synthesized with MgAC, which inhibited oxidation in aqueous solution [36]. Taking into consideration this MgAC function, MgAC can be expected to positively alter the properties of nZVI, and namely, enhance their stability and reactivity by wrapping of said nZVI particles.

Here, we report the studies of MgAC templated nZVI synthesis for nZVI stabilization in aqueous solution and discuss its feasibility for application to environmental clean-up of contaminated land. Specifically, nZVI was synthesized in a suspension of MgAC in order to produce stabilized nZVI particles. The ratio of MgAC to iron was varied in order to obtain variability of the particles and their surface coating. The stability of synthesized nZVI particles was characterized by sedimentation analysis, observation of particle size, and measurement of surface charge. Through stability assays, the effect of MgAC on nZVI stability is discussed with morphology analysis by transmission electron microscope (TEM) and X-ray diffraction (XRD). To investigate the relationship between the amount of MgAC and reactivity of the nZVI particles, assays of reactive iron content and reactivity toward nitrate reduction

Table 1
Conditions for MgAC template assisted nZVI synthesis in aqueous solution.

Fe concentration (g/L)	0.5						
[Fe ²⁺]:[BH ₄ ⁻] (mol:mol)	1:2.5						
MgAC concentration (g/L)	0	0.5	2.5	3.75	5	10	20
[MgAC]:[Fe] (w:w)	0	1	5	7.5	10	20	

were applied. All characterizations of the MgAC coated nZVI were compared to uncoated nZVI particles synthesized without MgAC. Based on the stability and reactivity tests with MgAC coated nZVI particles, the appropriate synthesis condition was determined. Subsequently, the stabilization mechanism and future aspects of suggested composite material for environmental cleanup is discussed.

2. Materials and methods

2.1. Chemicals

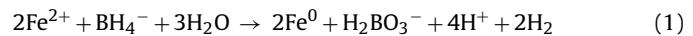
Ferrous sulfate heptahydrate ($\geq 99.0\%$), sodium borohydride ($\geq 98.0\%$), 3-aminopropyltriethoxysilane ($\geq 98.0\%$, denoted as APTES), potassium nitrate ($\geq 99.0\%$), hydrochloric acid (37%) were obtained from Sigma-Aldrich (St. Louis, MO, USA). Magnesium chloride hexahydrate ($\geq 99.0\%$) was purchased from Junsei Chemical Co., Ltd. (Tokyo, Japan) and bulk ethanol (95%, 18 L) was bought from Samchun Pure Chemicals (Pyeongtaek, Gyeonggi-do, Korea). Unless otherwise stated, all of the chemicals were used as received from the supplier. All solutions were prepared using degassed deionized water (DDIW) by purging with nitrogen gas for 3 h.

2.2. Synthesis of MgAC

For the preparation of MgAC, the protocol utilized was per previous studies [23,27–29]. Briefly, 8.4 g (~ 0.04 mol) of MgCl₂·6H₂O was dissolved with 200 mL of ethanol solution in a 500-mL beaker. After fully mixing for 30 min, 13 mL (~ 0.06 mol) of APTES was added to the solution drop-wise. Immediately, the reaction product formed white slurry. Subsequent magnetic stirring for 24 h yielded a complete sol-gel reaction; the white slurry was collected by centrifugation at 6000 $\times g$ for 15 min. The product was then washed repeatedly with ~ 200 mL of pure ethanol, in order to remove excess metals and impurities. The harvested product was dried at 50 °C for 24 h in an oven, and the dried solid materials were ground using a mortar and pestle prior to use in stock solution.

2.3. Synthesis of MgAC coated nZVI

In this study, the mild chemical reduction of metal salts in the solution phase was used to prepare nZVI, as stated in previous research [40]:



The synthesis of MgAC coated nZVI was conducted in a 250-mL three-open-neck round bottom flask reactor. The central neck was housed with a tunable mechanical stirrer at 40–2000 rpm (RZR2021, Heidolph, Germany). The stirring speed was adjusted to 250 rpm for nZVI synthesis, and to 100 rpm for aging. The desired amount of MgAC was dissolved in 100 mL of DDIW, and 50 mL of a ferrous (Fe(II)) solution (35.8 mM) was introduced to the MgAC solution. Then, 50 mL of sodium borohydride solution (89.6 mM) was introduced into the reactor to reduce the ferrous ion to nZVI. The concentrations of solutions were determined based on Eq. (1) and Table 1. Ferrous sulfate and sodium borohydride solutions were introduced via peristaltic pump with a constant delivery rate of 5 mL/min.

The nZVI was collected via centrifugation (4500 rpm, 10 min, Heraeus Multifuge X1, Thermo Fisher Scientific Inc., USA) of the solution, after an aging time of 25 min. The collected particles were then washed with 1 mM NaHCO₃ and immediately characterized and tested for reactivity. For the XRD analysis, the MgAC coated nZVI were dried in an anaerobic chamber (N₂:H₂ = 95:5, Coy laboratory products, USA) after removing excess water by absorbing it into filter paper and excess paper tissues.

2.4. Physical characterization

2.4.1. Morphological observation

Fresh nZVI and MgAC coated nZVI particles, as well as MgAC dispersed in aqueous solution, were characterized using a transmission electron microscope (TEM, Tecnai F20 model, Philips electron optics, Eindhoven, Netherlands). For preparation of the TEM samples, a droplet of diluted sample suspension was placed on a carbon-coated Cu grid (300-mesh), and immediately dried under anaerobic conditions for 12 h. For the elemental mapping of MgAC coated nZVI, an energy-dispersive X-ray spectroscopy (EDS) analysis was conducted [32].

2.4.2. XRD patterns and Fourier transform infrared (FT-IR) spectra

Crystalline structures related to MgAC coated nZVI was analyzed by means of micro-area X-ray diffraction (D/MAX-2500, Rigaku, 18 kW). The scan range was acquired for 3–80° 2θ with a scan speed of 1.2° min⁻¹. To examine the organo-functional groups of MgAC, Fourier transform infrared (FT-IR) spectra were recorded (FT-IR 4100, Jasco, Japan). For this, samples were prepared with 90 wt% of KBr and 10 wt% of the analyzed material using the KBr pellet mode [28,29].

2.4.3. Sedimentation analysis for examination of stability

Stability of as-prepared MgAC coated nZVI was determined by sedimentation analysis using a UV–Vis spectrophotometer (Cary 50, Agilent Technologies Inc., USA) [9,10]. The sedimentation rate was regarded as independent from solution viscosity, because the viscosity of MgAC coated nZVI slurry after washing did not vary significantly (1.15 ± 0.05 mPas at 25 °C). Freshly prepared samples were diluted with 1 mM NaHCO₃ to obtain identical initial absorbance of 2.25 ± 0.25 [14]. Evanoff and Chumanov [41] reported that the absorbance of metal nanoparticle suspension has relevance to the size of metal nanoparticles. In this study, the 'pre-grafting' of nZVI was applied so that the primary particle size could be manipulated. Consequently, the initial absorbance of nZVI suspension would be different when suspensions have same concentration. Therefore, in this study, the initial absorbance was chosen as an indicator of identical initial condition.

The dispersions were shaken but not sonicated prior to the experiment. Then, the samples were transferred into a 1-cm plastic cuvette and capped to prevent further oxidation during the sedimentation test. The absorbances of diluted samples were monitored as a function of time, with the optical absorbance at 508 nm, to obtain the sedimentation curve. The sedimentation curves were interpreted using the following equation, as suggested by Phenrat et al. [6].

$$I_t = I_0 e^{-t/\tau} \quad (2)$$

where I_t is the absorbance of solution at time t , I_0 is the initial absorbance, τ is the characteristic time which is related to the hydrodynamic radius of the particles by the following equation based on Stoke's law:

$$\tau = \frac{9\eta(\beta - p_f)}{2g^2(\rho_s - \rho_l)^2 R_H^2} \quad (3)$$

where η is the solvent viscosity, β is a function of the permeability of the fractal aggregate, p_f is the fluid pressure, ρ_s and ρ_l are density of solid and liquid, g is the acceleration due to gravity, and R_H is the hydrodynamic radius.

2.4.4. Particle size and zeta potential

The particle size was obtained by dynamic laser light scattering (DLS, Malvern Zetasizer NanoZS, USA), where the diluted sample (identical to that used in the sedimentation test) was applied for analysis. The scattered light intensity was detected by a photo detector at a scattering angle of 173°, consequently, size distributions were produced from the intensity measurements using an exponentially decaying, standard autocorrelation coefficient, which is related to the hydrodynamic radius through the Stokes–Einstein equation. Zeta potential measurements were also carried out, using the same DLS unit. All measurements were performed triplicate at room temperature.

2.5. Reactivity characterization

2.5.1. Reactive iron content

The reactive iron contents in as-prepared MgAC coated nZVs were determined by measuring the H₂ gas produced after acid digestion, as suggested by Liu et al. [42] with modification.



Five-mL quantities of concentrated hydrochloric acid (~37%) were transferred to 22 mL glass vials, which were then purged with nitrogen gas and capped. Five-mL quantities of as-prepared nZVI slurry were transferred by syringe through the PTFE septum, and allowed to react to completion for 24 h. Then, 0.2 mL of the headspace within the closed vial was taken by a gas-tight syringe and the H₂ content was determined by gas chromatography (Mikrolab GC82, Mikrolab Aarhus A/S, Denmark) using a 4.5 m × 3.0 mm stainless-steel column packed with molecular sieve 5A, using N₂ as a carrier gas and a thermal conductivity detector (TCD). The temperatures of the injector, detector, and column were maintained at 90 °C. Additionally, the total iron concentration in the acid digested solution was measured by an atomic absorption spectrometer (AAAnalyst 200, PerkinElmer, USA). Based on total iron and H₂ concentration, the content of reactive iron in the samples was calculated.

2.5.2. Nitrate reduction batch test

Batch tests for nitrate reduction were conducted in a 50-mL glass serum bottle. The bottle was filled with 36 mL of nZVI slurry washed with 1 mM NaHCO₃ and the solution was purged with nitrogen gas before the injection of nitrate stock solution. The initial pH of MgAC coated nZVI slurry was stable at pH 8.8 ± 0.2. After the bottle was tightly capped with PTFE/silicon septum and aluminium crimp seal, 4 mL of nitrate stock solution (1000 mg NO₃⁻-N/L) was injected to the bottle through the septum. The nominal concentrations were 100 mg NO₃⁻-N/L (6.14 mM) and 1000 mg Fe/L (17.92 mM), respectively. The bottle was mixed on a shaker at 100 rpm. Samples of 2 mL were taken periodically and filtered with 0.45 μm syringe filters, and immediately analyzed by ion chromatography (DX-1500, Dionex Co., Sunnyvale, CA, USA) with IonPac AS14 carbonate eluent anion-exchange column.

The reaction rate of the nitrate reduction was interpreted by the following pseudo-first-order kinetic:

$$C_t = C_{ss} + (C_0 - C_{ss})e^{-kt} \quad (5)$$

where C_t is the nitrate concentration at certain time, C_0 is the initial nitrate concentration, C_{ss} is the nitrate concentration after the nZVI

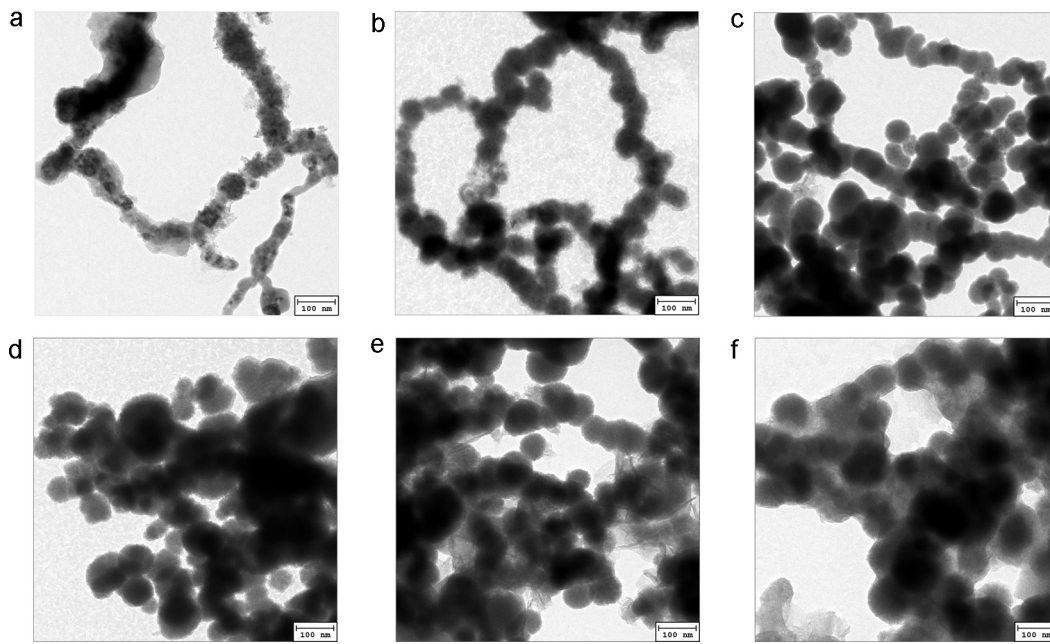


Fig. 1. Transmission electron microscopic (TEM) images of MgAC coated nZVI with different MgAC/Fe ratio. (a) 0 (bare nZVI), (b) 1.0, (c) 5.0, (d) 7.5, (e) 10, and (f) 20. Note that in (b) black arrows indicate MgAC particles.

is totally consumed, and k is the observed pseudo-first-order rate constant (h^{-1}).

3. Results and discussion

3.1. Properties of MgAC coated nZVI

Fig. 1 shows morphologies of uncoated nZVI, MgAC coated nZVI with different MgAC/Fe ratios (1.0, 5.0, 7.5, 10, and 20). Uncoated nZVI exhibited chain-linked and amorphous spheres as nanoclusters conventionally do (Fig. 1(a)), ranging from 30 to 100 nm, and with a broad particle size distribution corresponding to the previous results [43–47]. Interestingly, at low MgAC loadings (MgAC/Fe ratio of 1.0), MgAC adsorbed onto the surface of nZVI particles like a thin sheathed layer (Fig. 1(b)), with nZVI morphologies similar to uncoated nZVI. The more clear structure of spherical MgAC coated nZVI particles were observed at 5.0 of MgAC/Fe ratio, possibly by decreasing attraction between nZVI particles (Fig. 1(c)). However, with increased MgAC loading (7.5, 10, and 20), MgAC coating was thickened (Fig. 1(d)–(f)). Although pure spherical nZVI was reduced, the increase in coating of MgAC also increased the particles sizes, and MgAC acted as a bridge with nZVI particles, leading to large aggregated groupings. To observe the composition distribution of silica-sheathed nZVI particles in the composite at a ratio of 7.5, elemental mapping was displayed (Supplementary Figure S1). Which illustrated MgAC covered nZVI particles on the surface, with a homogeneous distribution of Mg, Si, and Cl elements sourced from Mg-aminoclay, composed of Mg (octahedral sheet), Si (sandwiched tetrahedral sheets), and Cl (counter ions for the stabilized amine groups). Certainly, the compositions of Fe was from nZVI surface and, and the presence of O stemmed from both MgAC and iron oxide on the nZVI shell surface [32].

The suggested coating mechanism of organo-building blocks of MgAC onto nZVI in aqueous solution is considered to be mainly electrostatic attraction between positively charged MgAC particles, in a wide pH range (pH 2.0–12.0), by protonated amine groups [35] and negatively charged zeta potential of nZVI particles at $>\text{pH } 8.1$ [48]. Synthesis of the nZVI occurred at a pH of approximately 9.6,

due to a pKa of 10.6 for MgAC [31]. As a result, the low concentration of MgAC during nZVI synthesis had a negligible effect on the synthesized nZVI morphology, as compared to uncoated nZVI. This indicates that after nucleation of nZVI, the organo-building blocks of MgAC were attached onto the surface of nZVI particles. In contrast, at high concentrations of MgAC, nucleation growth was inhibited by steric hindrance of MgAC. This limited magnetic attraction of each spherical particle, and immediately coated the nZVI particle surfaces. Notably, TEM examination of MgAC dispersed in aqueous solution, ranging from 30 to 150 nm diameter (Supplementary Figure S2), corresponding with findings in the literature [20]. For the consideration of thickness of MgAC in MgAC coated nZVI, MgAC led to a condensed and thin coating on the surface of the nZVI by electrostatic attraction.

For the confirmation of iron species and crystallinity of as-prepared MgAC coated nZVI, the crystalline patterns in XRD results are investigated for MgAC, uncoated nZVI, and MgAC coated nZVI (Fig. 2). MgAC shows poor crystalline phyllosilicate hybrid

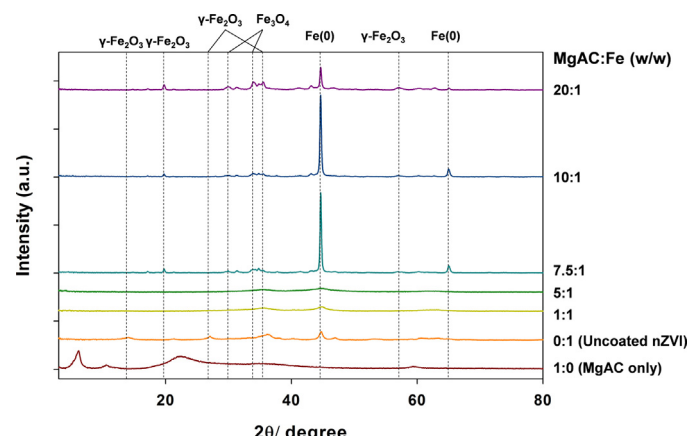


Fig. 2. Powder X-ray diffraction (XRD) patterns of MgAC, uncoated nZVI, and MgAC coated nZVI with different MgAC/Fe weight ratios.

organoclay: $2\theta = 6.10^\circ$, 10.50° , 22.70° , 35.47° , and 59.28° correspond to $d_{001} = 14.49 \text{ \AA}$, $d_{002} = 8.42 \text{ \AA}$, $d_{020,110} = 3.92 \text{ \AA}$, $d_{130,200} = 2.53 \text{ \AA}$, and $d_{060,330} = 1.56 \text{ \AA}$. The basal spacing of d_{001} and the existence of $d_{060,330}$ indicate the mesolamella layers and 2:1 smectite structure, respectively, in line with the literature [31]. Uncoated nZVI shows a Fe(0) core surrounded with an iron oxide shell of $\gamma\text{-Fe}_2\text{O}_3$ [45–47]. Meanwhile, the significant structural change was observed in the range of 5.0–7.5. The distinct Fe(0) peak was detected at MgAC/Fe ratio above 7.5, and it indicated the production of MgAC coated crystalline nZVI. This clear change of nZVI properties was also detected during stability and reactivity tests which would be described in following sections. Therefore, it was clear that the nZVI properties could be manipulated by the addition of MgAC in solution and the amount of MgAC should be controlled to have desired properties for environmental applications.

In addition, the organo-functional groups of MgAC were confirmed (Supplementary Figure S3): $-\text{OH}$ (3402 cm^{-1}), $-\text{CH}_2$ ($3040/2937 \text{ cm}^{-1}$), $-\text{NH}_3^+$ (2011 cm^{-1}), $-\text{NH}_2$ (1612 cm^{-1}), $-\text{CH}_2$ (1462 cm^{-1}), $-\text{Si}-\text{C}-$ (1139 cm^{-1}), $-\text{Si}-\text{O}-\text{Si}-$ ($1227/1139/1036 \text{ cm}^{-1}$), $-\text{CN}-$ (937 cm^{-1}), and $-\text{MgO}$ (563 cm^{-1}), resulting in organo-functional groups retained by coordination bonding to Mg metals. This matches well with the MgAC published in literature [27–29]. Thus, the novel nano-object of MgAC coated nZVI exhibited the presence of MgAC, which followed the self-assembling protocol under equilibrium conditions by the driving force of electrostatic attractions [18]. Particularly, as the peak intensities of protonated and amine groups were weaker, it might be expected that these organo-functional pendants strongly interacted with nZVI particles.

3.2. Effect of MgAC on particle stability

3.2.1. Sedimentation of MgAC coated nZVI

The FT-IR study revealed that the main functional groups of MgAC were: $-\text{CH}_2$, $-\text{NH}_2$, $\text{Si}-\text{O}$, and $\text{Si}-\text{O}-\text{metal}$; this corresponds to the ideal unit structure of MgAC. Among the functional groups, metal ions are reported to be well complexed with $-\text{NH}_2$ groups. Moreover, the non-protonated $-\text{NH}_2$ group in neutral or basic conditions is known to complex better with metal ions rather than $-\text{NH}_3^+$, which prevents the adsorption of metal cations onto MgAC [31,49,50]. Due to the high pKa value of MgAC, the pH of the synthesis mixture was higher than 9.0, which is favorable for metal ion adsorption on MgAC. As a result, Fe^{2+} can bind on the surface of MgAC by chelating with $-\text{NH}_2$ groups via hydrogen bonding and van der Waals forces. The bound Fe^{2+} can be reduced to Fe(0) by addition of a strong reductant (NaBH_4). Because the positively charged MgAC exhibit electrostatic repulsion, the individual MgAC coated nZVI particles remain dispersed as individual nZVI particles, rather than aggregated particles. In addition, due to the propagation in nZVI particle growth on the surface of the MgAC, resulting nZVI appeared to be disconnected grape-like structures, rather than necklace and chain-linked nanoclusters [51]. Depending on the applied amount of MgAC, the density and dimensions of surface coating by MgAC for nZVI synthesis in aqueous solution were altered, which significantly affect the growth and aggregation of nZVI.

The sedimentation profiles of synthesized MgAC coated nZVI with different MgAC/Fe weight ratios were obtained by optical absorbance. Inferences on the sedimentation behavior were evaluated based on the evolution characteristics of the optical absorbance of the suspensions over time. The normalized absorbance of suspensions with different amounts of MgAC is plotted in Fig. 3 as a function of time. Due to their large density and diameter, nZVI particles settle down; and consequently, there is a

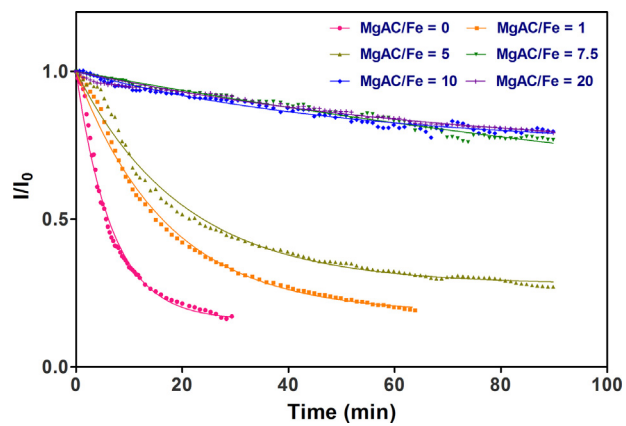


Fig. 3. Sedimentation patterns of as-prepared MgAC coated nZVI with different MgAC/Fe weight ratios. The curves were obtained by fitting the data to the sedimentation equation (Eq. (2)).

general tendency of normalized absorbance to decrease with time, due to the disappearance of nZVI from the illuminated region as sedimentation proceeds. Nevertheless, as can be observed, the rate of decrease of normalized absorbance, i.e., sedimentation rate, is lower for the MgAC coated nZVI suspensions than that for the uncoated nZVI.

As illustrated in Fig. 3, the weight ratio between MgAC and iron has significant effect on the sedimentation profile. The amount of MgAC exhibits a positive effect on the particle stability. The uncoated nZVI settled down very quickly, with obvious signs of a high tendency toward aggregation. The characteristic time, τ , was calculated from the sedimentation profile with modified Stokes equation, as suggested by Phenrat et al. (Eq. (2)) [6], and is presented in Fig. 4(a). According to the sedimentation profiles, the characteristic time increased from 6.71 to 83.8 min, with increased ratios of MgAC to iron. Significant change of characteristic time was observed between MgAC/Fe-ratios 5.0 and 7.5, thereafter no further significant difference with MgAC/Fe-ratios in the range of 7.5–20 was observed. The characteristic time is directly correlated with estimated hydrodynamic radius (Eq. (3)), where the increase of characteristic time clearly indicated the decrease of particle size in aqueous nZVI suspension.

3.2.2. Particle size of prepared MgAC coated nZVI obtained by dynamic light scattering (DLS)

Dynamic light scattering (DLS) is one of the most popular methods for particle size determination, especially for nano-particles. Shining a monochromatic light beam into a solution with spherical particles in Brownian motion causes a Doppler Shift when the light hits the moving particle(s), changing the wavelength of the incoming light; which is related to the size of the particle. In this study, the same diluted solutions that were used for sedimentation were applied for DLS measurement, then the trend and value was compared with the sedimentation test results.

Fig. 4(b) shows the obtained particle size measured by DLS. The particle size (diameter) decreased from 5132 to 186 nm in MgAC/Fe weight ratios of 0 and 20, respectively. Of note, the significant decrease of particle size was observed in the range of MgAC/Fe weight ratios 5.0–7.5. In comparison with sedimentation test results, the change of particle size in nm range could be detected more sensitively than with sedimentation. Even though the sensitivity was different between the methods, the overall trend was identical, which showed a very high positive linear relationship ($r^2 = 0.9855$, $p < 0.0001$).

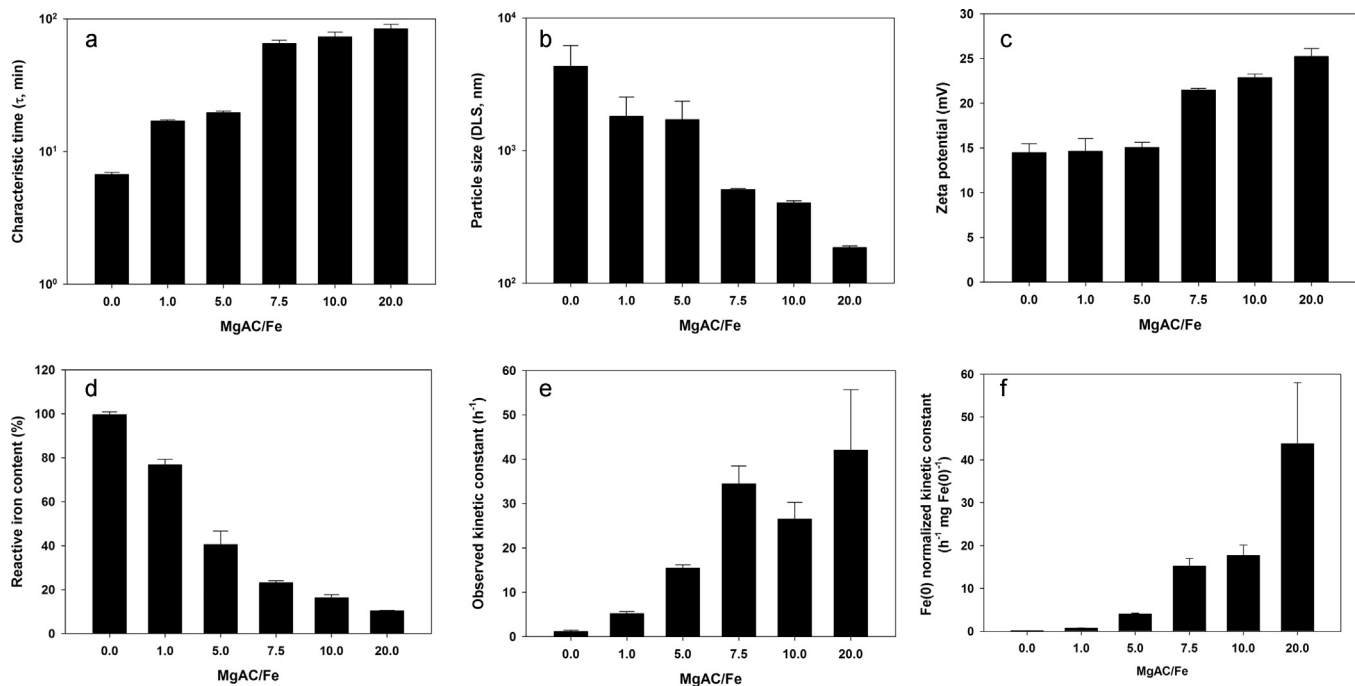


Fig. 4. Characteristics of MgAC coated nZVI with different MgAC/Fe ratios. (a) Calculated characteristic time from sedimentation test, (b) particle size from DLS measurement (diameter), (c) zeta potential, (d) reactive iron contents estimated from H_2 development by acid digestion, (e) pseudo-first-order kinetic constants for nitrate reduction, and (f) pseudo-first-order kinetic constants for nitrate reduction normalized to reactive iron content. T-bars indicate the standard deviation on each result.

3.2.3. Effectiveness of MgAC for nZVI stabilization and its mechanism

According to previous results on nZVI stability, MgAC showed feasibility as a stabilizing agent for nZVI synthesis. This stable nZVI could be synthesized with MgAC coating, and the stabilizing effect was mainly determined by the applied amount of MgAC. The optimal weight ratio between MgAC and iron was determined to be 7.5, based on stability testing. To investigate the stabilization mechanism of MgAC, the zeta potential was measured, as is illustrated in Fig. 4(c).

The zeta potential of uncoated nZVI was 14.5 mV, and the zeta potential gradually increased to 25.3 mV with increasing amounts of MgAC. An especially great increase of zeta potential was observed in the MgAC/Fe ratio range of 5.0–7.5, which coincides with the characteristic time and the particle size obtained by sedimentation and DLS, respectively. Therefore, it is clear that zeta potential could explain the stabilization effect of MgAC. The positively charged MgAC covers the surface of nZVI particles due to electrostatic interaction between MgAC and nZVI, whose interaction is stronger than the magnetic attraction of individual nZVI particles toward one another.

Stabilizing agents have been used to modify the surface of nZVI, with two different approaches, pre- and post-grafting. Generally, commercial nZVI has been stabilized by the post-grafting technique, which adds the stabilizing agent after nanoparticle synthesis [10,14]. Even though higher stability could be achieved by post-grafting, only aggregate size can be controlled, the primary particle properties cannot be controlled. In this study, the pre-grafting technique is applied to stabilize nZVI. The stabilizing agent solution was applied during nZVI synthesis; therefore, the primary particle size could be controlled by inhibition of nZVI nuclei growth. This pre-grafting technique alters the primary characteristics of the nZVI, not only stability and mobility, but also the reaction rate and mechanisms. The performance of MgAC as a stabilizing agent is comparable with previously applied various organic polymers in pre-grafting techniques [4,52].

3.3. Effect of MgAC on nZVI reactivity

Despite the stability increase by the stabilizing agent, it should be considered that some stabilization approaches have been shown to decrease reactivity. The decreased reactivity has been attributed to a number of mechanisms, including the blocking of reaction sites on the surface of nZVI by the coating created by the stabilizing agents, inhibiting the diffusion of aqueous phase contaminant to the surface. The slow diffusion of reaction products away from the surface may inhibit desorption from reactive sites. However, the loss of reactivity must be weighed against benefits of stability provided by the surface coating.

The reactivity of nZVI was determined by nitrate reduction batch test with iron-limiting conditions. Theoretically, the nitrate reduction by nZVI could be explained by the following equation, as suggested by Alowitz and Scherer [53]:



Based on the stoichiometry, 1000 mg/L of nZVI can reduce 62.8 mg/L of NO_3^- ; although the 1000 mg/L of nZVI is not enough to reduce all of nitrate in the solution, which contains 100 mg NO_3^- /L, this iron-limiting condition is suitable to determine the nitrate reduction capacity of the prepared nZVI.

Fig. 5 gives the reduction of nitrate expressed as the ratio of nitrate concentration (C) at a given time to that at the beginning of the experiment (C_0), as a function of reaction time. The low reaction rate of uncoated nZVI is attributed the aggregation of uncoated nZVI during the synthesis and washing steps. The aggregation is inevitable during the synthesis without a stabilizing agent, and it can change the overall structure of nZVI and its accessible surface area; which in turn changes its reaction rate and reaction efficiency, making it more difficult for nitrate to come in contact with the inside of the large aggregated nZVI. Ryu et al. [54] reported the effect of sonication on nitrate reduction rate, and that sonication showed a positive effect on the nitrate reduction rate, due to aggregate destruction by sonication; thereafter a fresher surface

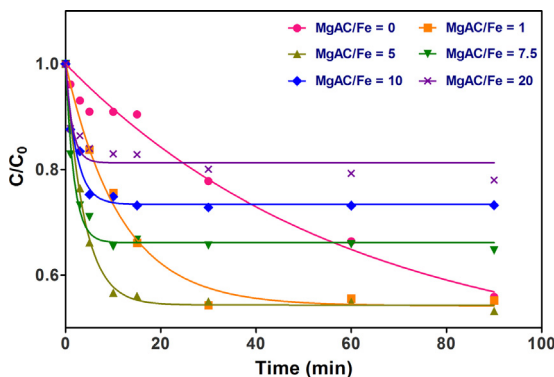


Fig. 5. Nitrate reduction profiles with different MgAC/Fe ratios. The curves were obtained by fitting the data to the pseudo-first-order kinetic described by Eq. (5).

can react with nitrate. It clearly demonstrated that aggregation is an important factor to determine the reactivity of nZVI.

On the other hand, this aggregation and dispersion problem was not significantly raised with MgAC. A sharper decrease of nitrate in the initial period (0–15 min) was observed with MgAC addition. In the presence of MgAC, production of a more dispersed aggregate can have a larger surface area exposed to the aqueous phase. As such, the higher reduction rate and larger accessible surface area is expected. After reaction for 30 min, the nitrate concentration plateaued, and it clearly demonstrated the capacity of prepared nZVI for nitrate reduction. The prepared nZVI with MgAC weight ratio between 1.0 and 5.0 showed similar nitrate reduction capacity as uncoated nZVI. However, lower nitrate reduction capacity was observed in nZVI prepared with high MgAC/Fe ratios, even though the nitrate reduction in the initial period was faster. This phenomenon was observed at the weight ratios of 5.0 and 7.5, which is the region of significant change in stability. Therefore, it is clear that the prepared nZVI characteristics, including stability and nitrate reduction capacity, were dramatically affected in this region.

It is assumed that the nitrate reduction capacity is closely related with the produced zero valent state of iron, Fe(0). To confirm this, the reactive iron content was determined by acid digestion, followed by measurement of hydrogen production. The hydrogen content in the sealed vial was measured, and it indicated a decreased content of zero valent iron with increasing MgAC/Fe weight ratios, which is in agreement with the observed nitrate reduction capacity. This indicates that the reactive iron content varies with the amount of applied MgAC, which should be considered for the kinetics analysis.

Nitrate reduction kinetic rates were obtained by pseudo-first-order kinetics. The reaction constants are presented in Fig. 4. Fig. 4(e) illustrates the reaction constant without consideration of the reactive iron content. Generally, the reaction constants increased with applied amount of MgAC ($1.17\text{--}42.0\text{ h}^{-1}$). Especially, the Fe(0) normalized kinetic constants, presented in Fig. 4(f), exhibited a high positive linear relationship with the amount of MgAC ($r^2 = 0.9593$, $p < 0.0001$). The normalized reaction constant increased from 0.124 to $43.8\text{ h}^{-1}\text{ mg-Fe(0)}^{-1}$. The high reduction rate is possibly attributed to the discrete distribution of individual nZVI particles, which provide a more accessible surface than aggregated nZVI. Moreover, the well-dispersed MgAC coated nZVI corroded faster, thereby showing higher reactivity for nitrate reduction.

It was reported that the stabilizing agent for post-grafting led to reduced reactivity when compared to uncoated nZVI [9], where the reaction rate decreased with increasing amounts and concentrations of stabilizing agent. This negative impact of stabilizing agent was explained as competitive adsorption and site

blocking by adsorbed modifiers. However, negative impact was not observed in the case of MgAC, even though the reduction capacity was influenced by reactive iron content. Faster nitrate reduction was observed due to dispersed and positively charged MgAC coated nZVI, which can attract the nitrate anion easily. It is known that adsorption precedes nitrate reduction by nZVI; therefore, the attractive force by surface charge is important for the nitrate reduction kinetics [40].

Furthermore, the lower reduction capacity should be considered for subsequent implementation of a prepared nano-composite. Exactly the same reaction conditions for the synthesis, i.e. time and concentrations, were applied for each synthesis batch; though the applied amount of MgAC was varied. A Fe(II)-aminoclay complex might require more time or reductant for complete reduction, however, it was not considered in this study. In a previous study, the effect of synthesis conditions, i.e. time and concentrations, showed a profound impact on the characteristics of nZVI [40]. Moreover, Gu et al. reported that excessive borohydride is crucial for obtaining a high Fe(0) yield from nZVI synthesis [15]. Apparently, at lower $\text{NaBH}_4/\text{Fe(III)}$ ratios (< 10), incomplete reduction of exchangeable iron was achieved, which manifested lower reaction efficiencies. If more borohydride or longer Fe^{2+} reduction time would be used in the synthesis, more Fe^{2+} would presumably be reduced to Fe(0). Therefore, the effect of synthesis conditions on reactive iron content will be investigated as further research.

4. Conclusion

For the first time, stable MgAC coated nZVI was prepared, and was found to have higher stability and reactivity versus uncoated nZVI. The particle size could be manipulated by the applied amount of MgAC relative to iron; and the optimal weight ratio between MgAC and iron was determined to be 7.5, based on stability testing by sedimentation analysis and DLS. Both methods showed a high positive linear relationship. The particle (aggregate) size decreased 96% to 186 nm (in diameter). The morphology change with different MgAC loading was investigated with TEM and XRD. As MgAC loading increased, nZVI particle growth was inhibited and thin sheathed grape-like nZVI particles with a higher degree of crystallinity were produced. The higher stability of MgAC coated nZVI could be explained by the higher zeta potential in the stable MgAC coated nZVI particles, which suggests that the stabilization mechanism was increased electrostatic repulsion obtained from the positively charged MgAC coating.

Moreover, the MgAC coated nZVI exhibited higher reactivity to target contaminants. The higher reaction rate toward nitrate, observed ($1.17\text{--}42.0\text{ h}^{-1}$) and Fe(0) normalized ($0.124\text{--}43.8\text{ h}^{-1}\text{ mg-Fe(0)}^{-1}$), shown in this study directly verified the advantages of nano-sizing iron, which increase the overall reaction speed. The stabilized MgAC coated nZVI prepared in this study, therefore, showed high feasibility to be applied in subsurface contamination remediation, where it is desired to have high mobility in the subsurface and short required time to degrade contaminants.

Acknowledgements

Yuhoon Hwang acknowledges funding for this study through a H.C. Ørsted Postdoc Program stipend from Technical University of Denmark and Basic Science Research Program through the National Research Foundation of Korea (NRF) funded by the Ministry of Education, Science and Technology (2013R1A6A3A03026864). Henrik R. Andersen and Paul D. Mines received funding from the Technical University of Denmark (DTU) for this work through a strategic research initiative for cooperation with KAIST. Also this work was

supported by Inha University Research Grant (INHA-47290). We thank Jin Seok Choi of the KAIST Research Analysis Center for the TEM imaging.

Appendix A. Supplementary data

Supplementary material related to this article can be found, in the online version, at <http://dx.doi.org/10.1016/j.apcatb.2013.10.017>.

References

- [1] D. O'Carroll, B. Sleep, M. Krol, H. Boparai, C. Kocur, *Adv. Water. Resour.* 51 (2013) 104–122.
- [2] R.A. Crane, T.B. Scott, *J. Hazard. Mater.* 211–212 (2012) 112–125.
- [3] C.B. Wang, W.X. Zhang, *Environ. Sci. Technol.* 31 (1997) 2154–2156.
- [4] F. He, D. Zhao, *Environ. Sci. Technol.* 41 (2007) 6216–6221.
- [5] N. Sakulchaicharoen, D.M. O'Carroll, J.E. Herrera, *J. Contam. Hydrol.* 118 (2010) 117–127.
- [6] T. Phenrat, N. Saleh, K. Sirk, R.D. Tilton, G.V. Lowry, *Environ. Sci. Technol.* 41 (2007) 284–290.
- [7] X.-q. Li, D. Elliott, W.-x. Zhang, *Crit. Rev. Solid State Mater. Sci.* 31 (2006) 111–122.
- [8] P.G. Tratnyek, R.L. Johnson, *Nano Today* 1 (2006) 44–48.
- [9] N. Saleh, K. Sirk, Y. Liu, T. Phenrat, B. Dufour, K. Matyjaszewski, R.D. Tilton, G.V. Lowry, *Environ. Eng. Sci.* 24 (2007) 45–57.
- [10] N. Saleh, H.-J. Kim, T. Phenrat, K. Matyjaszewski, R.D. Tilton, G.V. Lowry, *Environ. Sci. Technol.* 42 (2008) 3349–3355.
- [11] H.-J. Kim, T. Phenrat, R.D. Tilton, G.V. Lowry, *Environ. Sci. Technol.* 43 (2009) 3824–3830.
- [12] F. He, D. Zhao, *Environ. Sci. Technol.* 39 (2005) 3314–3320.
- [13] H. Dong, I.M. Lo, *Water Res.* 47 (2013) 419–427.
- [14] A. Tiraferri, K.L. Chen, R. Sethi, M. Elimelech, *J. Colloid Interface Sci.* 324 (2008) 71–79.
- [15] C. Gu, H. Jia, H. Li, B.J. Teppen, S.A. Boyd, *Environ. Sci. Technol.* 44 (2010) 4258–4263.
- [16] H. Jia, C. Wang, *Environ. Technol.* 34 (2013) 25–33.
- [17] D. Li, C. Li, K. Suzuki, *Appl. Clay Sci.* 77–78 (2013) 56–60.
- [18] S. Mann, *Nat. Mater.* 8 (2009) 781–792.
- [19] K.K.R. Datta, A. Achari, M. Eswaramoorthy, *J. Mater. Chem. A* 1 (2013) 6707–6718.
- [20] A.J. Patil, S. Mann, *J. Mater. Chem.* 18 (2008) 4605–4615.
- [21] M.G. da Fonseca, E.C. da Silva Filho, R.S.A. Machado Junior, L.N.H. Arakaki, J.G.P. Espinola, C. Airoldi, *J. Solid State Chem.* 177 (2004) 2316–2322.
- [22] A.S.O. Moscofian, C.T.G.V.M.T. Pires, A.P. Vieira, C. Airoldi, *RSC Adv.* 2 (2012) 3502–3511.
- [23] Y.-C. Lee, E.S. Jin, S.W. Jung, Y.-M. Kim, K.S. Chang, J.-W. Yang, S.-W. Kim, Y.-O. Kim, H.-J. Shin, *Sci. Rep.* 3 (2013), 1292 (1–8).
- [24] J.L. Vickery, S. Thachepan, A.J. Patil, S. Mann, *Mol. Biosyst.* 5 (2009) 744–749.
- [25] S.C. Holmstrom, A.J. Patil, M. Butler, S. Mann, *J. Mater. Chem.* 17 (2007) 3894–3900.
- [26] A.J. Patil, M. Li, E. Dujardin, S. Mann, *Nano Lett.* 7 (2007) 2660–2665.
- [27] W. Farooq, Y.-C. Lee, J.-I. Han, C.H. Darpito, M. Choi, J.-W. Yang, *Green Chem.* 15 (2013) 749–755.
- [28] Y.-C. Lee, B. Kim, W. Farooq, J. Chung, J.-I. Han, H.-J. Shin, S.H. Jeong, J.-Y. Park, J.-S. Lee, Y.-K. Oh, *Bioresour. Technol.* 132 (2013) 440–445.
- [29] Y.-C. Lee, Y.S. Huh, W. Farooq, J. Chung, J.-I. Han, H.-J. Shin, S.H. Jeong, J.-S. Lee, Y.-K. Oh, J.-Y. Park, *Bioresour. Technol.* 137 (2013) 74–81.
- [30] Y.-C. Lee, Y.S. Huh, W. Farooq, J.-I. Han, Y.-K. Oh, J.-Y. Park, *RSC Adv.* 3 (2013) 12802–12809.
- [31] Y.C. Lee, E.J. Kim, D.A. Ko, J.-W. Yang, *J. Hazard. Mater.* 196 (2011) 101–108.
- [32] Y.-C. Lee, S.-J. Chang, M.-H. Choi, T.-J. Jeon, T. Ryu, Y.S. Huh, *Appl. Catal. B: Environ.* 142–143 (2013) 494–503.
- [33] Y.-C. Lee, E.J. Kim, J.-W. Yang, H.-J. Shin, *J. Hazard. Mater.* 192 (2011) 62–70.
- [34] Y.-C. Lee, J.-W. Yang, *J. Ind. Eng. Chem.* 18 (2012) 1178–1185.
- [35] P. Chaturbedy, D. Jagadeesan, M. Eswaramoorthy, *ACS Nano* 4 (2010) 5921–5929.
- [36] K.K.R. Datta, C. Kulkarni, M. Eswaramoorthy, *Chem. Commun.* 46 (2010) 616–618.
- [37] A.S. Kumar, K.K. Datta, T.S. Rao, K.V. Raghavan, M. Eswaramoorthy, B.V. Reddy, *J. Nanosci. Nanotechnol.* 12 (2012) 2000–2007.
- [38] A. Achari, K.K. Datta, M. De, V.P. Dravid, M. Eswaramoorthy, *Nanoscale* 5 (2013) 5316–5320.
- [39] K.K.R. Datta, M. Eswaramoorthy, C.N.R. Rao, *J. Mater. Chem.* 17 (2007) 613–615.
- [40] Y.-H. Hwang, D.-G. Kim, H.-S. Shin, *Appl. Catal. B: Environ.* 105 (2011) 144–150.
- [41] D.D. Evanoff, G. Chumanov, *J. Phys. Chem. B* 108 (2004) 13957–13962.
- [42] Y. Liu, S.A. Majetich, R.D. Tilton, D.S. Sholl, G.V. Lowry, *Environ. Sci. Technol.* 39 (2005) 1338–1345.
- [43] Y.-C. Lee, C.-W. Kim, J.-Y. Lee, H.-J. Shin, J.-W. Yang, *Desalin. Water Treat.* 10 (2009) 33–38.
- [44] J. Shin, Y.-C. Lee, Y. Ahn, J.-W. Yang, *Desalin. Water Treat.* 50 (2012) 102–114.
- [45] Z.H. Ai, L.R. Lu, J.P. Li, L.Z. Zhang, J.R. Qiu, M.H. Wu, *J. Phys. Chem. C* 111 (2007) 4087–4093.
- [46] Z. Ai, L. Lu, J. Li, L. Zhang, J. Qiu, M. Wu, *J. Phys. Chem. C* 111 (2007) 7430–7436.
- [47] T. Luo, Z. Ai, L. Zhang, *J. Phys. Chem. C* 112 (2008) 8675–8681.
- [48] Y.-P. Sun, X.-Q. Li, W.-X. Zhang, H.P. Wang, *Colloids Surf. A: Physicochem. Eng. Asp.* 308 (2007) 60–66.
- [49] L. Zhang, C. Yu, W. Zhao, Z. Hua, H. Chen, L. Li, J. Shi, *J. Non-Cryst. Solids* 353 (2007) 4055–4061.
- [50] A. Dong, J. Xie, W. Wang, L. Yu, Q. Liu, Y. Yin, *J. Hazard. Mater.* 181 (2010) 448–454.
- [51] L. Lu, Z. Ai, J. Li, Z. Zheng, Q. Li, L. Zhang, *Cryst. Growth Des.* 7 (2007) 459–464.
- [52] T. Long, C.A. Ramsburg, *J. Hazard. Mater.* 189 (2011) 801–808.
- [53] M.J. Alowitz, M.M. Scherer, *Environ. Sci. Technol.* 36 (2002) 299–306.
- [54] A. Ryu, S.-W. Jeong, A. Jang, H. Choi, *Appl. Catal. B: Environ.* 105 (2011) 128–135.